SCIENTIFIC REPORTS

OPEN

Extracellular matrix stiffness regulates human airway smooth muscle contraction by altering the cell-cell coupling

Received: 2 September 2018
Accepted: 13 June 2019
Published online: 02 July 2019

Samuel R. Polio[1], Suzanne E. Stasiak[1], Ryan R. Jamieson[1], Jenna L. Balestrini[3], Ramaswamy Krishnan[2] & Harikrishnan Parameswaran[1]

For an airway or a blood vessel to narrow, there must be a connected path that links the smooth muscle (SM) cells with each other, and transmits forces around the organ, causing it to constrict. Currently, we know very little about the mechanisms that regulate force transmission pathways in a multicellular SM ensemble. Here, we used extracellular matrix (ECM) micropatterning to study force transmission in a two-cell ensemble of SM cells. Using the two-SM cell ensemble, we demonstrate (a) that ECM stiffness acts as a switch that regulates whether SM force is transmitted through the ECM or through cell-cell connections. (b) Fluorescent imaging for adherens junctions and focal adhesions show the progressive loss of cell-cell borders and the appearance of focal adhesions with the increase in ECM stiffness (confirming our mechanical measurements). (c) At the same ECM stiffness, we show that the presence of a cell-cell border substantially decreases the overall contractility of the SM cell ensemble. Our results demonstrate that connectivity among SM cells is a critical factor to consider in the development of diseases such as asthma and hypertension.

Asthma, Crohn's disease, and hypertension are widespread chronic diseases that affect the airways, the gut, and blood vessels respectively. Although they are very different diseases, physiologically they share one common feature: they are all characterized by excessive narrowing of the luminal area of a hollow, tubular organ. Traditionally, these changes have been viewed as a disease of the smooth muscle (SM) and treatment strategies have focused on identifying and targeting molecular pathways that control force generation inside the SM cell[1–4]. However, it is becoming increasingly clear that the etiology of excessive narrowing of airways and blood vessels cannot be explained by considering the SM cell in isolation from its native environment[5–10]. In order to generate enough force to effect a change in the luminal area, the contractile apparatus of individual SM cells must physically connect with each other to form a force transmission pathway that wraps around the circumference of the tube. Clearly, the number of SM cells that form this connected path as well as the stiffness of the cell-cell and cell-extracellular matrix interactions will dictate how much luminal constriction is achieved for a given level of SM activation. Currently, we know very little about how these connections among SM cells are achieved in a multicellular SM ensemble.

At the cellular level, SM cells can form direct connections with their neighboring cells through cadherin-mediated adherens junctions[11]. They can also connect to the extracellular matrix (ECM) through integrin-mediated focal adhesions[12]. Focal adhesions allow SM cells to indirectly connect with other SM cells over long distances through the ECM[13,14]. As such, SM cells *in vivo* have multiple options available to them to make connections among themselves and transmit their force. The factors that dictate the choice of force transmission pathways used by SM cells in healthy and diseased tissue are still unclear. Both focal adhesions and adherens junctions are mechanosensitive structures through which cells can respond to, and probe the stiffness and ligands present in their surrounding environment. Focal adhesion size and maturation rates have been shown to depend on cytoskeletal tension[15] and ECM stiffness[16]. Similarly, in cell-cell cadherin junctions, the cadherin-catenin

[1]Department of Bioengineering, Northeastern University, Boston, MA, 02115, USA. [2]Department of Emergency Medicine, Beth Israel Deaconess Medical Center, Boston, MA, 02115, USA. [3]Department of Biomedical Engineering, Yale University, New Haven, CT, USA. Correspondence and requests for materials should be addressed to H.P. (email: h.parameswaran@northeastern.edu)

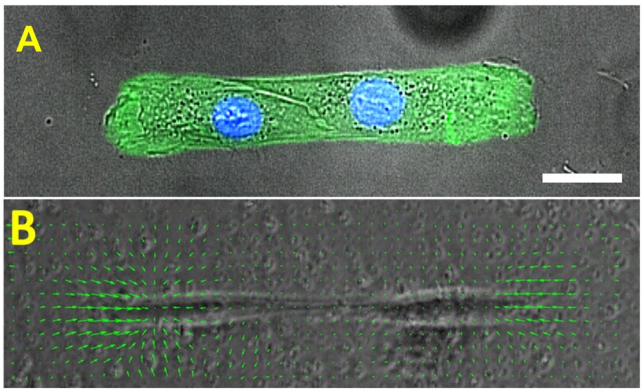

Figure 1. (**A**) shows a composite image with a phase contrast image of a two-ASM cell ensemble superimposed on fluorescent images of their nuclei stained in blue using DAPI. The 150 μm × 15 μm rectangular micro-pattern on the Nusil gel surface is marked using fluorescent gelatin (green). The scale bar is 25 μm. (**B**) shows the displacement field (green arrows) calculated from the movement of 1 μm beads spin-coated on the gel surface. The displacement field is superimposed on the phase contrast image of the two-SM cell pair. The stiffness of the substrate is E = 300 Pa.

complex/actin filament binding in adherens junctions has been shown to exhibit catch bond characteristics up to 10pN after which it transitions into a slip bond[17]. Based on these data, we hypothesize that mechanical cues such as ECM stiffness can alter the nature of force transmission pathways (cell-cell vs cell-ECM) in a multicellular ensemble of human SM cells.

To test this hypothesis, we applied ECM micropatterning techniques to create islands of two human airway smooth muscle (ASM) cells and measured the effect of changing ECM stiffness on the ASM force transmitted through cell-cell coupling[18,19]. To determine the stiffness of the ECM in healthy human airways, we measured the Young's modulus (E) of airway tissue isolated from decellularized human lung tissue. We found that the stiffness of airway ECM was size dependent with small airways having lower values of E. For airways with inner diameter <3 mm, which are known to collapse in asthma[20], the E was of the order of 100 Pa. We report direct measurement of forces exerted by an ASM cell on its neighbor, and on the ECM for substrates with stiffness matching healthy (E = 300 Pa) and remodeled tissue (E = 13 kPa). On soft substrates matching the ECM stiffness of healthy human airways, we find that ASM cells exert more of their longitudinal tension on their neighboring ASM cells compared to the ECM. Imaging reveals the presence of well defined adherens junctions connecting ASM cells indicating that there is strong coupling between the cells in healthy tissue. As the substrate stiffness is increased to match that of remodeled tissue, ASM-ASM coupling weakens and more of the ASM force is exerted on the matrix. Imaging confirms the gradual loss of adherens junctions and replacement by focal adhesions as the ECM stiffens. These experiments indicate that the ECM stiffness can act as a switch that regulates whether forces are transmitted via the ECM or through cell-cell contacts. The change in connectivity can also significantly change the overall contractile strength of the ensemble. Excessive contraction of airways and blood vessels can therefore emerge as a result of change in connectivity among SM cells driven by extracellular matrix remodeling. Our results highlight the need to develop new therapies for asthma and hypertension that target extracellular matrix remodeling.

Results

Creating a two-cell ensemble of human airway smooth muscle cells. In order to measure the forces that SM cells exert on their neighbor and on the ECM, we adapted an experimental system that has been previously described for similar measurements in cardiac myocytes[18]. Briefly, the method involves creating a rectangular shaped "micro tissue" with exactly two cells in contact with each other. In the case of ASM cells, we wanted the cells to be elongated and aligned in a manner that was consistent with how ASM cells are organized *in vivo*[21]. To this end, we used a novel UV activated ECM patterning technique (Primo, Alvéole, France) to create rectangular shaped islands of gelatin on a polydimethylsiloxane (PDMS) substrate[22]. To facilitate measurement of cellular traction forces, a layer of fluorescent beads was spin-coated on the surface of the gel substrate prior to gelatin patterning. The PDMS substrate material used in this study was NuSil[23], an optically clear, non-porous material whose stiffness can be tuned in the range Young's modulus, E = 300 Pa–40 kPa. A substrate stiffness of E = 300 Pa was used to mimic the ECM stiffness of healthy human airways. With the onset of airway remodeling, there is collagen deposition in the airways and the stiffness of the ECM increases[24]. A substrate stiffness of E = 13 kPa was used to mimic remodeled ECM. The length of the rectangular pattern of gelatin was specified to match the length of ASM cells plated on non-patterned NuSil gels (150 μm) and the breadth (15 μm) was set by trial and error to allow for enough space within the rectangle to fit exactly two ASM cells. Figure 1A shows a composite image with the phase contrast image of a two-ASM cell ensemble on E = 300 Pa superimposed on fluorescent images of their nuclei stained in blue using DAPI and the 150 μm × 15 μm rectangular micro-pattern of the Nusil gel surface using fluorescent gelatin (green). A phase contrast image of a two ASM cell ensemble on E = 300 Pa with displacement fields generated from the fluorescent beads overlaid on top is shown in Fig. 1B. We found that these dimensions (150 μm × 15 μm) gave the cells enough area to spread and form a well-defined

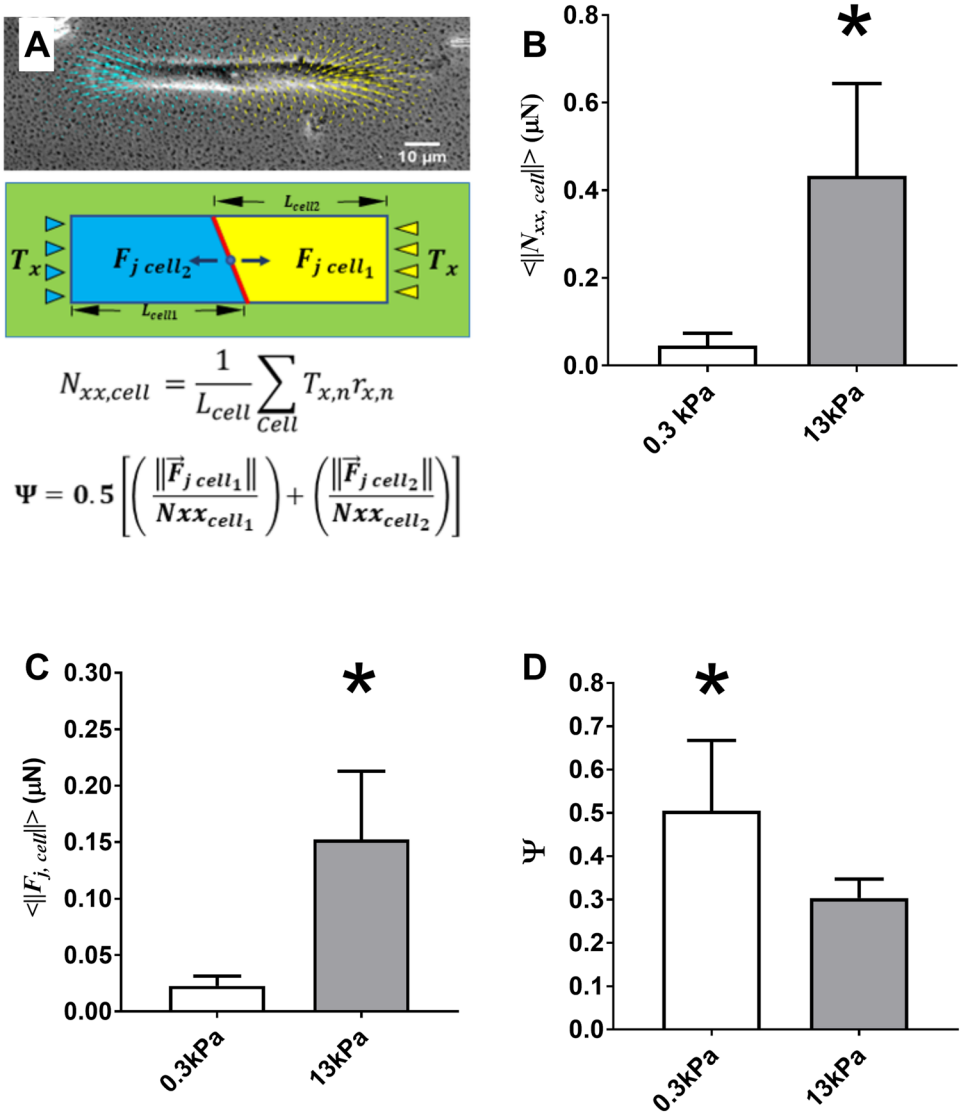

Figure 2. (**A**) The phase contrast image shows a two ASM cell pair, the traction field generated by this "micro-tissue" is split in two (yellow for $cell_1$ and blue for $cell_2$) by manually outlining each cell in the image. The force exerted on the cell-cell junction but each cell $\vec{F}_{j\ cell}$ can be calculated as the unbalanced traction force in that cell. **(B)** The average magnitude of the longitudinal tension of ASM cells in our two-cell ensemble $\langle \|N_{xx,\ cell}\| \rangle$ ($p \leq 0.001$; $N = 8$, Mann-Whitney). **(C)** Average magnitude of the force exerted at the cell-cell junction $\langle \|\vec{F}_{j,\ cell}\| \rangle$ ($p < 0.001$; $N = 8$, Mann-Whitney). **(D)** Strength of the coupling between the two ASM cells, Ψ calculated using equation (3) ($p < 0.05$; $N = 8$, t-test). The height of each bar represents the mean value and the error bar represents the standard deviation of the measurements.

border between them. A detailed description of the protocols used for cell culture, gel manufacture and the ECM micro-patterning can be found in the Methods section.

ASM-ASM coupling strength decreases with increasing ECM stiffness. Using the beads embedded in the NuSil gel, we measured traction forces exerted by the two-cell ensemble of ASM cells on the substrate. To measure the forces exerted by each ASM cell on its neighbor, we manually outlined the cell-cell junction from phase contrast images and used this to separate the two-ASM cell ensemble into two distinct regions corresponding to each ASM cell. (Fig. 2A). This allowed us to directly calculate the force exerted by each cell on the cell-cell junction $\vec{F}_{j\ cell}$ as the unbalanced traction force in each cell[19,25].

$$\vec{F}_{jcell_i} = -\sum_{cell_i} \vec{T}_n \tag{1}$$

where $\vec{F}_{j\ cell_i}$ is the force exerted by the i^{th} cell ($i = 1, 2$) on the cell-cell boundary. $\vec{T}_n$ is the traction force vector corresponding to computational grid n within the i^{th} cell. The average magnitude of the force exerted on the

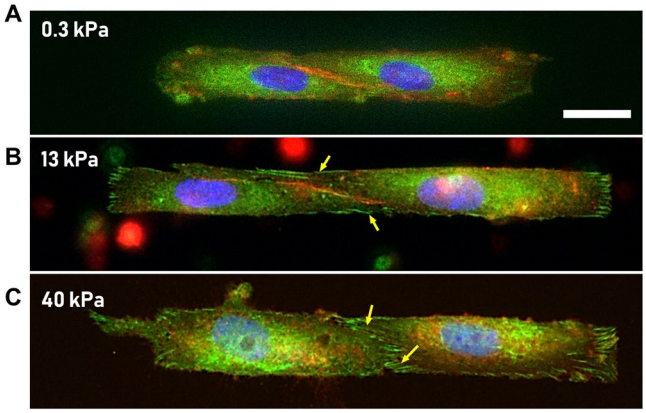

Figure 3. (**A**–**C**) ASM cells were stained for β-catenin (an adherens junction marker; red), Vinculin (focal adhesion marker; green), and the nucleus (DAPI; blue). Scale bar is 10 μm. (**A**) Healthy ECM, E = 300 Pa: ASM-cells form stable cell-cell junctions and the boundary is clearly marked by β-catenin stain. (**B**,**C**) Remodeled, stiffer ECM (E = 13 kPa–40 kPa): As the ECM stiffness increases to 13 kPa, one sees the appearance of focal adhesions near the cell-cell boundary (marked by yellow arrows). When ECM stiffness is further increased to 40 kPa, the ASM-ASM boundary (red) gives way to cell ECM focal adhesions (green).

cell-cell junction, $\langle \| \overrightarrow{F}_{j\ cell_1}, \overrightarrow{F}_{j\ cell_2} \| \rangle$ is plotted in Fig. 2C for healthy (E = 300 Pa) and remodeled ECM (E = 13 kPa). We found that as the ECM stiffness increases, the force on the cell-cell junction increased significantly from 0.023 ± 0.01 μN (N = 8) to 0.152 ± 0.06 μN (N = 8) ($p < 0.001$, Mann-Whitney). In Fig. 2B, we show changes in the average longitudinal tension of the ASM cells, N_{xx} as defined by

$$Nxx_{cell} = \frac{1}{L_{cell\ Cell}} \sum T_{x,n} r_{x,n} \tag{2}$$

In our two-cell pairs at E = 300 Pa and 13 kPa, $\langle \| N_{xx,\ cell} \| \rangle$ increases significantly from 0.05 ± 0.03 μN (N = 8) at 300 Pa to 0.43 ± 0.21 μN (N = 8) at 13 kPa ($p < 0.001$, Mann-Whitney). Several previous studies have noted that cellular traction forces increase with the increase in ECM stiffness[26,27]. Figure 2B confirms that within the range of ECM stiffness that is of interest to this study, changing ECM stiffness increases ASM cellular tractions significantly. Consequently, the force exerted on the cell-cell junction $\langle \| \overrightarrow{F}_{j\ cell_1}, \overrightarrow{F}_{j\ cell_2} \| \rangle$ is not a reliable indicator of cell-cell coupling strength, as this quantity will always increase as traction forces $\| \overrightarrow{T}_n \|$ increase. To normalize for this effect, we calculate a dimensionless ratio (Ψ) which is indicative of the mechanical coupling between cells[18] and is defined as:

$$\Psi = 0.5 \left[\left(\frac{\| \overrightarrow{F}_{jcell_1} \|}{Nxx_{cell_1}} \right) + \left(\frac{\| \overrightarrow{F}_{jcell_2} \|}{Nxx_{cell_2}} \right) \right] \tag{3}$$

In these calculations, the *x*-axis was assumed to be aligned with the long axis of the rectangular pattern with the origin at the cell-cell border such that $r_x = 0$ at the cell-cell junction. The length of the cell L_{cell} was measured manually from phase contrast images as the length parallel to the *x-axis* (the direction in which the ASM cells are aligned). From equation (3), the ASM-ASM coupling strength, Ψ is a dimensionless ratio which measures the fraction of the cell's longitudinal tension that it exerts on the boundary. The variable Ψ can vary continuously between 0 and 1, where Ψ = 0 indicates that the cells exert all their longitudinal tension on the matrix and Ψ = 1 indicates that the cells exert all their longitudinal tension on the cell-cell boundary. For ASM cells, Ψ decreased significantly from 0.51 ± 0.16 (N = 8) to 0.31 ± 0.04 (N = 8) ($p < 0.05$, t-test, power ≥ 0.8) as substrate stiffness was increased from 300 Pa to 13 kPa (Fig. 2D) indicating that the ASM cells can potentially physically decouple from each other as ECM stiffness is increased. To verify this result, we imaged the cells after fluorescently staining for markers of cell-cell and cell-ECM adhesion.

Cell-cell adherens junctions are progressively replaced by cell-ECM focal adhesions as airway ECM stiffness increases. To verify our mechanical measurements of cell-cell coupling strength, we imaged our two-ASM cell ensembles after staining for β-catenin (an adherens junction marker), vinculin (focal adhesion marker), and the nucleus (DAPI). Images of cells stained at three different stiffnesses are shown in Fig. 3. On substrates mimicking ECM stiffness of healthy tissue E = 300 Pa (Fig. 3A), the border between ASM cells is well defined by the β-catenin stain indicating the presence of adherens junctions at the ASM-ASM cell border. As ECM stiffness increases to E = 13 kPa, well defined focal adhesions (green: Fig. 3B) start to develop at the ASM-ASM cell border (yellow arrows in Panel B). This structural change is reflected in our mechanical measurements of Ψ which indicate a significant decrease in cell-cell coupling strength (Fig. 2). At E = 40 kPa, the

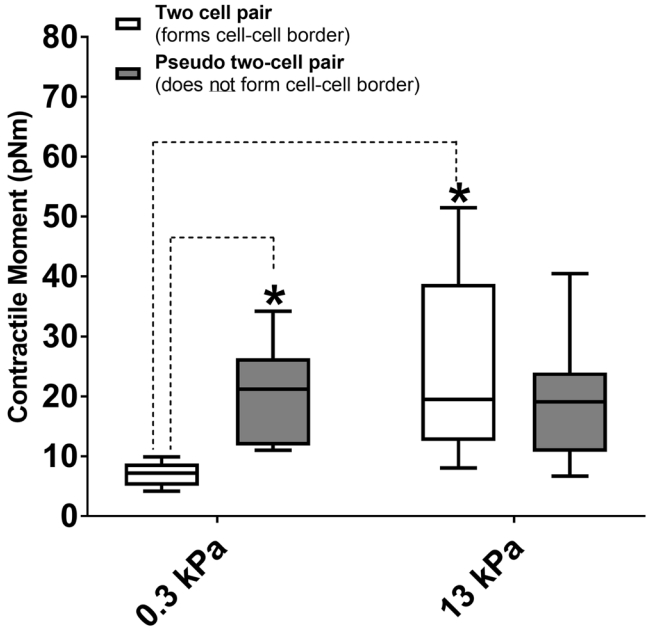

Figure 4. The contractile moment of a two-ASM cell ensemble is compared to that of a theoretical two-cell pair which does not form adherens (cell-cell) junctions. At E = 300 Pa, (healthy ECM), the theoretical pair of two ASM cells with no cell-cell connections has statistically higher contractile moment than the two-cell pairs which form cell-cell borders ($p < 0.05$, N = 8, Tukey test). At E = 13 kPa, the difference in contractile moment between the experimental two-cell pair and the theoretical pair is no longer statistically significant ($p = 0.379$, N = 8, Tukey test). The net contractile moment of the experimental two-cell ensemble does increase significantly with increase in ECM stiffness from E = 300 Pa to E = 13 kPa (N = 8, Tukey test, $p < 0.05$). Data is presented as a box-whisker plot. The box represents the 25, 50 (median) and 75 percentiles of the contractile moments. The whiskers represent the min and max of the contractile moments.

adherens junctions and the cell-cell border completely disappear, and focal adhesions can be seen at the border (yellow arrows Fig. 3C). Now, the two ASM cell ensemble separates into two individual ASM cells that are connected to the ECM. There is no functional border (of adherens junctions) between the ASM cells at E = 40 kPa. It should be noted that vinculin can also appear in adherens junctions, but if it does, it would spatially co-localize with β-catenin—which is not the case here. Hence, we can be certain that the vinculin (green) in Fig. 3A–C represents focal adhesions. Further, measurement of total area occupied by focal adhesions at the cell-cell border showed a statistically significant increase as E was increased from 0.3 kPa to 13 kPa from $49.3 \pm 3.7\,\mu m^2$ (N = 5) to $80.7 \pm 9.1\,\mu m^2$ (N = 5) ($p < 0.05$, t-test, power ≥ 0.9) confirming the qualitative visual observations from the fluorescent images in Fig. 3A,B.

Clarifying the confounding effect of ECM stiffness on the interpretation of data. Our results thus far give a strong indication that in a remodeled extracellular environment, the ASM cells change their connectivity from ASM-ASM connections to ASM-ECM connections and the net force of the ASM ensemble increases significantly. However, there is considerable evidence that changes in ECM stiffness can also influence cell mechanics even in single cells[28–30], and so cell-ECM interactions can be a potential confounding factor in interpreting our experimental findings. To isolate the effect of ASM-ASM coupling from ASM-ECM coupling on our results, we needed an independent means to verify that, *at the same ECM stiffness*, an ensemble of ASM cells that form strong adherens junctions among themselves would behave differently from an ensemble of adjoined ASM cells that do not form cell-cell adherens junctions at all. In other words, we wanted to find out whether the formation of adherens (cell-cell) junctions between cells in an ensemble would influence their overall contractility. Experimentally disrupting the cell-cell border[25,31] by calcium depletion or knock down of β-catenin affect cell viability and introduces additional confounding factors. Therefore, we constructed a simple mechanical equivalent of a two-ASM cell ensemble with no cell-cell contacts. In order to do this, we considered isolated, single ASM cells cultured on the rectangular patterns as before. The traction fields for each single cell were first calculated independently. Then, we translated the coordinate system from the two independent traction force vector fields, such that the two ASM cells were adjoint and aligned in the same direction. The vector fields at matching grids were added up vectorially to create the new traction field of this theoretical ensemble. We then calculated the contractile moment of this theoretical two-cell pair (which represents a two-cell pair with no cell-cell junctions) and compared this to the experimental data at 300 Pa and 13 kPa (Fig. 4) using a two-way ANOVA with ECM stiffness as one independent factor and the pseudo-two cell vs experimental two-cell pairs as the other independent factor. The ANOVA was followed by a pairwise comparison using the Tukey test.

We found that at E = 0.3 kPa (healthy ECM, where the ASM-ASM cell coupling was maximum: see Figs 3A and 2D), a connected two ASM cell ensemble has statistically significantly lower contractile strength (7.03 ± 2.0

pNm, N = 8) in comparison to two non-interacting ASM cells (20.19 ± 8.3 pNm, N = 8) $p < 0.05$, Tukey test; (Fig. 4). This shows that ASM-ASM connections via adherens junctions are not merely a pathway for transmitting ASM force. Adherens junctions allow the contractile apparatus of individual cells to interact in such a way that the contractile strength of a multicellular ensemble is significantly lower than an equivalent ensemble which connects through cell-ECM focal adhesions rather than cell-cell adherens junctions. Comparing these results to the same scenario on E = 13 kPa (remodeled ECM, where the ASM-ASM coupling was significantly lower. see Figs 3B and 2D), the contractile moment of a connected two ASM cell ensemble (24.7 ± 15.2 pNm, N = 8) was not statistically different from that of two non-interacting ASM cells (20.2 ± 8.3 pNm, N = 8, p = 0.356; Tukey test). As ASM-ASM coupling decreases, each ASM cell in the ensemble starts to behave like a single cell connected to a stiffer ECM and the net contractile moment increases significantly.

Measurement of ECM stiffness in healthy human airways. Airway segments (N = 13) with inner diameter ranging from 1.2 mm to 4.5 mm were dissected from decellularized human lungs for measurement of ECM stiffness. Each airway segment (labeled 2 in Fig. 5A) was threaded through a triangular piece of stainless-steel wire as shown in Fig. 5A and kept suspended between a lever arm (model 300B, Aurora scientific, dual mode muscle lever system; labeled 1 in Fig. 5A) and a force transducer (CSM-LC01, CSM instruments, Needham MA; labeled 3 in Fig. 5A) and kept suspended in an organ bath containing phosphate buffered saline maintained at 37 °C. The movement of the lever arm and the recording of forces generated was done using a laptop running custom software. The recorded forces were low-pass filtered at 10 Hz and sampled at a rate of 30 Hz. This system allows the decellularized airways to be stretched uniaxially in a way that simulates radial distension of the airway. Each airway segment was first preconditioned by applying three triangular displacement signals peaking at 40% macroscopic strain (ε_M) at a rate of 0.75 s^{-1}. The segments were then stretched to 100% strain and the corresponding force was recorded. Following the force measurements, the length of the airway segment, its inner diameter and wall thickness was measured from images taken using a light microscope (DinoLite LM ADT-413T). The force (F) generated by the decellularized airways upon stretching was used to calculate airway wall stress, $\sigma = F/2wl$; where w and l, are the wall thickness and length of the airway segment respectively. Strain, ε was defined as $\varepsilon = (d - d_0)/d_0$ were d is the displacement imposed by the lever arm and d_0 is the baseline inner diameter of the airway segment. Force-length and stress-strain curves for an airway with inner diameter of 1.8 mm are shown in Fig. 5B,C respectively. The stiffness of the airway ECM was evaluated as the Young's modulus $E(\varepsilon) = d\sigma/d\varepsilon$.

Airway ECM stiffness decreases with airway size. Our measurements of airway ECM stiffness are listed in Table 1. Hyperpolarized He MRI studies[20] have shown that the airways that constrict in response to agonist challenge in asthmatics are small airways with inner diameter less than 2.4 mm[20]. These airways had extremely soft ECM with E~O(100 Pa). Further, for airways with E ≤ 2 kPa, stiffness of the ECM appears to show a dependence on inner diameter of the airway, with smaller airways having lower values of ECM stiffness than larger airways(Fig. 5D). The dotted line is a linear regression with an R^2 of 0.61. The P-value indicates that the slope is significantly different from zero. A detailed discussion of the limitations that come with using decellularized human tissue can be found in the Discussion section of this manuscript.

Discussion

It is well understood by now that diseases such as hypertension, asthma and Crohn's are also accompanied by a substantial change in the extracellular matrix that surrounds, and connects to the smooth muscle cells[32]. The impact of such matrix remodeling on the excessive luminal narrowing of airways and blood vessels is not well understood. In this study, we measured the effect of ECM stiffness on the mechanical coupling between smooth muscle cells. We found that at low ECM stiffness mimicking healthy airway ECM (E = 300 Pa), ASM cells form cell-cell adherens junctions which create a well-defined border between the cells. Our force measurements showed that there is a strong mechanical coupling between the SM cells in the two-cell ensemble at this stiffness (Figs 2D and 3A). These findings are inline with independent reports that the recruitment of β-catenin to N-cadherin is an integral part of the force transmission machinery in healthy airways[11]. As ECM stiffness was increased (E = 13 kPa), we found that there was a significant decrease in cell-cell coupling strength. Imaging confirmed a gradual loss of cell-cell adherens junctions in favor of cell-ECM focal adhesions with increased ECM stiffness. On very stiff ECM (E = 40 kPa), the cell-cell border completely disappeared and well-defined focal adhesions were observed. These measurements show that ECM remodeling can not only increase the force generated by the individual SM cells but also alter the connectivity among cells within the smooth muscle layer, with cells favoring a force transmission pathway that runs through the ECM.

Currently, there are no measurements of ECM stiffness of healthy human airways in the literature. Here, we present measurements of ECM stiffness of healthy human airways made from decellularized human airways from a nonsmoker with no history of lung disease. The methods used to decellularize the tissue are described in the Methods section. We fully acknowledge that decellularization of tissue is not a perfect method. The technique used here is designed to minimize the tradeoff between cell removal and preservation of critical matrix components[33]. Our measurements of Young's modulus of the airway ECM is O(1 kPa). Healthy human airways have a Young's Modulus O(10 kPa)[34]. However, given the near circumferential alignment of smooth muscle cells around an airway[21] and the huge drop in stiffness of ASM cells following cytochalasin treatment[35], it is not surprising that ASM cells contribute significantly to the overall stiffness of the airway. In our study, we were limited by the availability of human lung tissue. If we did have access to human airway tissue, a better approach to characterize the stiffness of the airway ECM would have been to measure its Young's modulus after treatment with cytochalasin D or any other actin depolymerizing agent. These measurements would have provided the upper bound on the stiffness of human airway ECM, while avoiding the uncertainty that comes with decellularization. Even in this approach, there are some additional confounding effects to consider. Many ECM constituents (e.g. collagen) are

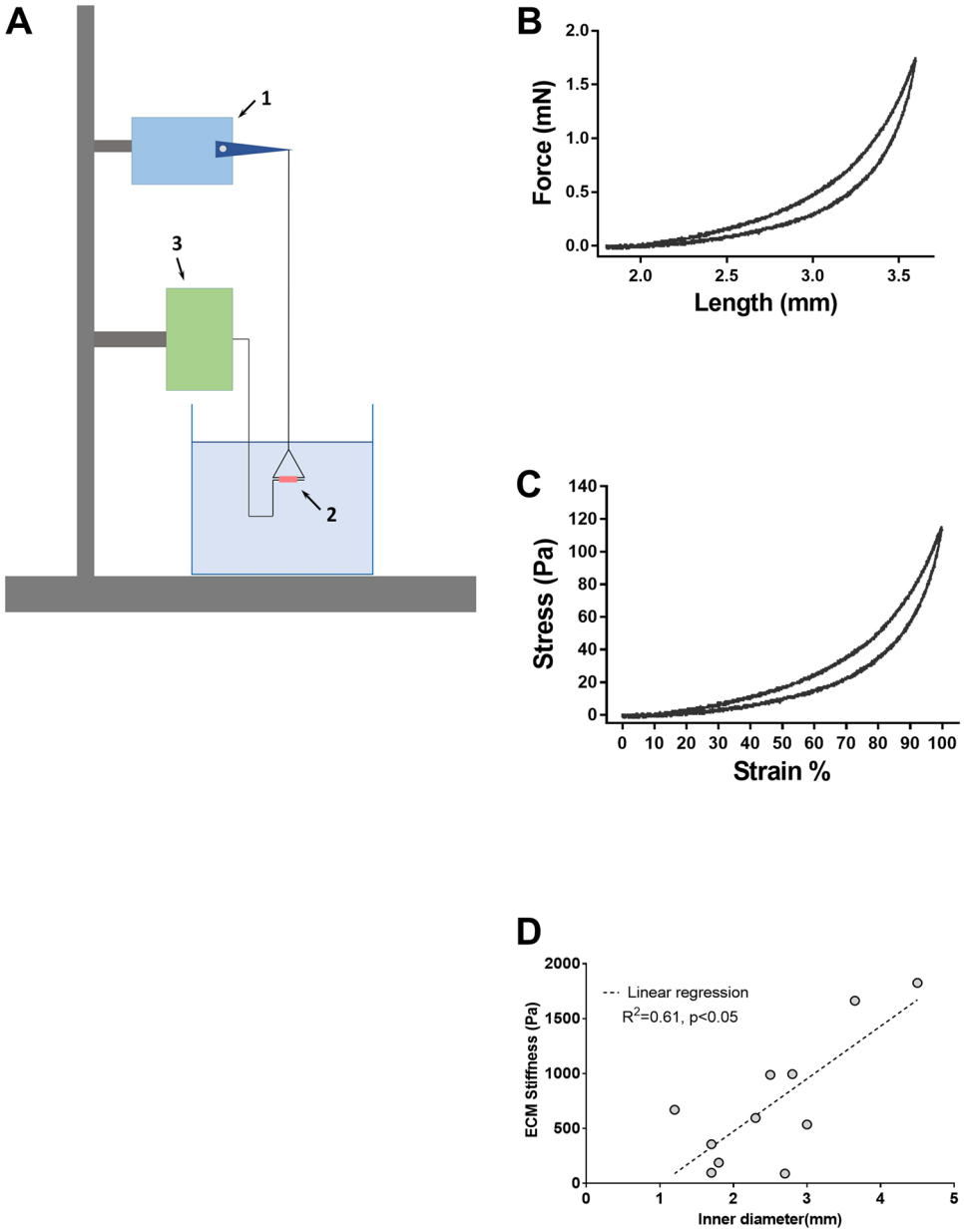

Figure 5. (**A**) shows the experimental setup used to measure the Young's modulus of airway ECM. Each airway segment (labeled 2/photograph shown) was threaded through a triangular piece of stainless-steel wire. The tissue is stretched using a lever arm (labeled 1) and the force generated was measured using a force transducer (labeled 3). **(B)** The force-length curve measured for a small airway **(C)** the corresponding stress-strain curve. **(D)** For airways with $E \leq 2$ kPa, the stiffness of the ECM appears to show a dependence on inner diameter of the airway, with smaller airways having lower values of ECM stiffness than larger airways. The dotted line is a linear regression with an R^2 of 0.61. The P-value indicates that the slope is significantly different from zero.

nonlinearly elastic. When cells are present, they will prestress the ECM, and increase the ECM stiffness. So the ECM stiffness actually felt by cells invivo will depend on cellular traction forces.

As the ECM was stretched, its stiffness showed a sharp increase for strains beyond 80%. During tidal breathing ($P_{tm} = 5cmH_20–10cmH_20$) airways typically operate close to the maximum diameter they can achieve[36]. On a stress-strain curve, this would correspond to the point at which the stiffness shows a sudden and dramatic increase. Since this occurred in our samples at 80% strain, the value of Young's modulus at 80% strain was chosen as the stiffness of the human airway ECM. Currently, there are no measurements of asthmatic airway ECM stiffness described in the literature. We make the assumption that ECM stiffness increases with the onset of asthma. This is a reasonable assumption given what we know about ECM remodeling in asthma[32]. We also note that several previous studies which examined changes in ASM mechanics with ECM stiffness also assume an increase in ECM stiffness with the onset of asthma[26,27].

Tissue Number	Inner Diameter (mm)	Young's modulus, E (Pa)
1	1.8	189.02
2	1.7	97.01
3	2.8	995.27
4	3.65	1662.8
5	2.5	988.13
6	3	536.19
7	2.3	596.02
8	2.7	89.54
9	3	6568.6
10	1.2	670.86
11	3.6	4866.12
12	4.5	1825.13
13	1.7	357

Table 1. Measurements of human airway ECM stiffness.

The role of ECM remodeling in the development of airway hyperrresponsiveness is unclear. Proteoglycans, for example, can oppose airway constriction due to the charged nature of their side chains. So, the increased proteoglycan deposition seen in moderate asthma[37] could play a protective role in asthma. However, remodeling of ECM components such as fibrillar collagens within the ASM layer can act to facilitate airway constriction if the changes increase the stiffness of the interconnects between ASM cells. Here, we wanted to understand whether changes in connectivity among SM cells at the same ECM stiffness could alter the overall contractile properties of the multicellular SM ensemble. This is extremely difficult (if not impossible) to test experimentally without introducing additional confounding effects[25,31]. Hence, we created a virtual mimic of our two-cell ASM ensemble by repositioning two isolated single ASM cells to create an aligned dipole with no cell-cell contacts. Our results demonstrate that even at the same ECM stiffness, a change in connectivity among cells within the smooth muscle layer from cell-cell contacts to cell-ECM contacts would increase the overall contractile strength of the SM ensemble. While the method of using a theoretical two-cell pair is appropriate and accurate for the calculation of contractile moments, we do acknowledge the limitations that come with the theoretical nature of this calculation.

Here we interpret the increase in traction force of the cell as an increase in cell contractility. A concern was raised during peer review as to whether the observed increase in traction with increase in ECM stiffness was a result of increased number of connections (focal adhesions) between the cell and the matrix as opposed to an increase in the cytoskeletal tension. The development of cellular force and formation of focal adhesions are tightly correlated processes[15] which cannot be separated from one another. The binding of integrins to the ECM has been found to show catch bond characteristics[38] where the bond lifetime increases with force. The same is true for linker proteins critical for the formation of focal adhesions such as Zyxin[39].

Our studies were limited to a two-cell ensemble system. *In vivo*, the airway SM cells are organized as a single layer of cells that spiral around the airways with a spiral pitch angle of 10 degrees[21,40]. These cells are constantly subjected to periodic stretch associated with tidal breathing and deep breaths. Modeling studies show that the connected nature of a smooth muscle ensemble can influence how the airway responds to deep breaths[41]. The extent to which fluctuating levels of stretch might impact our primary findings is therefore of great interest but is beyond the scope of the current work. Another area of future interest is to understand how SM cells respond to both contractile and relaxant stimuli. To this end, we are combining our approaches with concomitant measurements of pharmacological changes, to be performed in high-throughput, as is enabled by contractile force screening[23,42].

Here we used a novel UV based ECM patterning technique to create rectangular islands of gelatin on which we plated ASM cells to create our two-cell ensemble[22]. The technique was able to accurately reproduce a prescribed pattern on a PDMS substrate with a resolution down to 2 microns. We also used a newly developed PDMS substrate, NuSil instead of polyacrylamide (PAA) gels which are commonly used in traction force microscopy measurements. NuSil has several advantages compared to PAA gels. NuSil allows for direct photopatterning of ECM proteins on its surface as opposed to an indirect transfer of protein using glass coverslips[43,44]. NuSil is also nonporous and optically clear (refractive index ~1.4). Most importantly, the stiffness of these substrates could be tuned within a range of Young's modulus E = 300 Pa-40 kPa which allowed us to mimic the stiffness of healthy and remodeled human airway ECM stiffness. A detailed characterization of the mechanical properties of NuSil gels can be found in Yoshie *et al.*[23].

In this study, we found that increasing ECM stiffness from E = 300 Pa to 13 kPa results in loss of cell-cell adhesions and weakening of the cell-cell coupling between airway smooth muscle cells. Comparing this result to previously published measurements in other cell types, the present findings appear to be cell-type dependent. Our results are consistent with disruption of bovine, canine and human endothelial cell monolayers due to substrate stiffening[45,46], but not with measurements that show an increase in cell-cell coupling observed in myocardiocytes with an increase in matrix stiffness[18]. The cadherin-catenin complex/actin filament bonds that are at the core of cell-cell contacts have lifetimes that depend on force in a biphasic manner. The bond lifetimes increase with force up to 10pN (catch bonds/cell-cell adhesion is stabilized by force), after which the bond lifetimes decrease

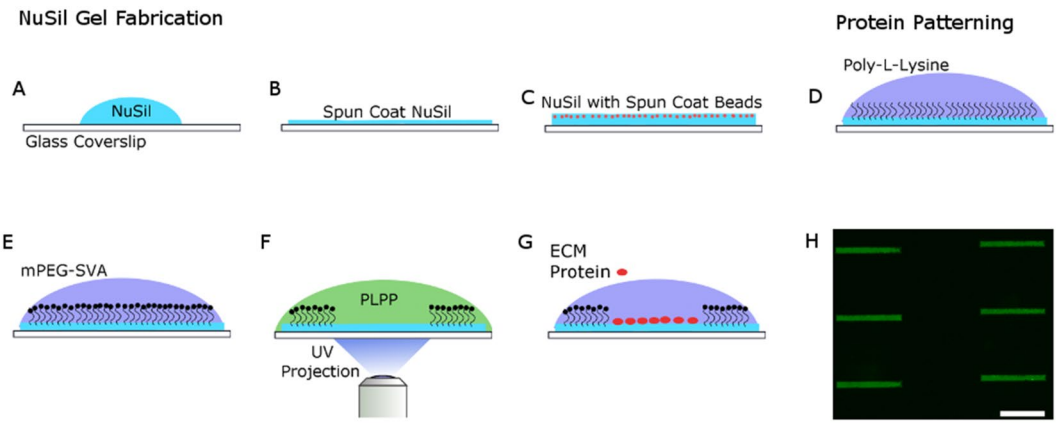

Figure 6. Schematic of the process used to create rectangular patterns of ECM proteins. (**A**) NuSil is spun coat onto a glass coverslip to create an even layer of gel on the surface of the cover slip as shown in panel (B). The NuSil is then baked overnight on an even surface at 60 °C. The process can be repeated with the addition of fluorescent beads to create a uniform, thin layer of beads as shown in panel (C). The surface is then coated with PLL (panel D) and then PEG-SVA (panel E), which forms amide bonds to PLL, preventing cell adhesion outside the desired patterned area and to the PLL itself. **(F)** The desired pattern, a 15 μm × 150 μm rectangle, is then projected using UV light (λ = 375 nm) onto the surface of the NuSil gel in the presence of PLPP, which helps to rapidly degrade the PLL-PEG coating in the exposed area. (**G**) The desired ECM protein is then added to the surface of the gel and then rinsed to only adhere to the UV exposed area. **(H)** shows a representative image of 150 × 15 μm rectangular patterns of fluorescent gelatin. Scale bar is 100 μm.

with increasing force (slip bonds/cell-cell adhesion is destabilized by force)[17]. This suggests that it is reasonable to expect the cell-cell coupling strength (Ψ) to depend on the contractility of cells considered, the range of ECM stiffness, the composition of the ECM and the specific focal adhesion & cell-cell adhesion proteins expressed in each cell type. We also note the complementary nature of cell-cell and cell-ECM contacts expressed by SM cells in an ensemble. A decrease in the area occupied by cadherin based cell-cell junctions was always accompanied by an increase in the total area occupied by focal adhesions. This observation is consistent with previous studies in other adherent cell types[47].

In most existing models of luminal constriction[48,49], the smooth muscle cells are lumped into one continuous layer in the cylindrical wall that generates the tension necessary for constricting the lumen while the extracellular matrix acts as the load against which the muscle constricts. In reality, these smooth muscle cells are organized in bundles and are able to dynamically adjust their connectivity with each other depending on extracellular mechanical factors such as matrix stiffness[21,40]. Here we have shown that the ECM stiffness can act as a switch that regulates whether forces are transmitted via the ECM or through cell-cell contacts. The change in connectivity can also significantly change the overall contractile strength of the ensemble. Excessive contraction of airways and blood vessels can therefore emerge as a result of change in connectivity among SM cells driven by extracellular matrix remodeling. Our results highlight the need to develop new therapies for asthma and hypertension that target extracellular matrix remodeling.

Methods

Fabrication of NuSil Gel. NuSil (NuSil Silicone Technologies, Carpinteria, CA) parts A and B were mixed in a 1:1 ratio (by volume). An appropriate volume of part B crosslinker (V/V) from Sylgard 184 (Dow Corning, Midland, MI) kit was added to the solution to increase substrate stiffness to desired levels. The relationship between substrate stiffness and % of Sylgard 184 part B crosslinker to be added can be found in Yoshie 2018[23]. In our study 0.36% (V/V) of Sylgard 184 part B was added to create substrates with E = 13 kPa. Approximately 1 mL of the mixture was placed on top of a 30 mm coverslip and was spun coat onto the surface at 800RPM (Fig. 6A,B). Next, the coated coverslip was baked in an oven overnight at 60 °C. Coverslips could then be coated with a thin layer of NuSil containing 1 μm fluorescent beads for traction force microscopy (Fig. 6C). The thin NuSil layer with beads was created by adding 1 mL solution of 2 μm fluorescent beads in a silicone solution (courtesy of Allen J. Ehrlicher, McGill University, Montreal, Canada) to the NuSil solution of a stiffness matching mixture. About 500 μL of solution was added to the surface of the gel and spun coat at 2600RPM. The bead coated coverslip was again baked in an oven overnight at 60 °C.

Photopatterning NuSil. NuSil gels were photopatterned using the Primo (Alveolé, Paris, France) micropatterning system. A schematic of the patterning process is illustrated in Fig. 6. The NuSil was coated with 0.1% Poly-L-Lysine (PLL; Sigma Aldrich, St. Louis, MO) for 1 h at room temperature (Fig. 6D). After, the PLL was rinsed 3x with 1x PBS at pH7.2, followed by 3x of 10 mM HEPES buffer at pH 8.2. Then, mPEG-SVA, MW 5kD (Laysan Bio; Arab, AL) was diluted to 50 mg/mL in 10 mM HEPES buffer at pH 8.2. The solution was added to the surface of gel and incubated for 1 h (Fig. 6E). After incubation, the surface was rinsed with PBS. Then, PLPP at a concentration of 14.5 mg/mL (Alveolé) was added to the surface of the gel prior to patterning. The UV system was used to pattern 15 μm × 150 μm at a dosage of 1700 mW/mm^2 (Fig. 6F) for traction force experiments. After

patterning, the gel was then rinsed with 1xPBS and incubated with 0.1% gelatin (ECM protein used here) for 1 h (Fig. 6G). The samples were washed with 1x PBS, leaving gelatin only in the area patterned. A typical pattern obtained using this protocol is shown in Fig. 6H. Samples were then stored in the refrigerator until seeded.

Cell Culture & Seeding Cells on Gel. Primary human airway smooth muscle cells (HASMCs) were acquired through the Gift of Hope Foundation (via Dr Julian Solway, University of Chicago). This is a publically available source and the donor remains anonymous and cannot be identified directly or indirectly through identifiers linked to the subject. This study meets NIH guidelines for protection of human subjects and no informed consent is necessary from this vendor as all donor identifiers are removed. All protocols used were carried out in accordance with the relevant guidelines and regulations that were reviewed and approved by the Institutional Biosafety Committee, Northeastern University. Cells were grown at 37 °C and 5% CO_2 and utilized prior to passage 7 for traction force experiments and for staining experiments. Cells were cultured in 10% fetal bovine serum, DMEM/F12, 1x penicillin/streptomycin, 1x MEM non-essential amino acid solution, and 250 µg/L Amphotericin B. Prior to measuring traction forces, the HASMCs were incubated in serum free medium for a minimum of 24 hours. The serum free medium was comprised of Ham's F-12 media, 1x penicillin/streptomycin, 50 µg/L Amphotericin B, 1x L-glutamine, 1.7 mM $CaCl_2$, 1x Insulin-Transferrin-Selenium Growth Supplement (Corning Life Sciences; Tewksbury, MA), and 12 mM NaOH.

Cell Traction Experiment. The protein coated gels were placed into 35 or 40 mm interchangeable coverslip dishes (Bioptechs, Butler, PA). The gels were UV sterilized for 30 mins. Cells were seeded at a density of 2400 cells/well in 10% serum media for 15 mins. After 15 mins, non-adherent cells were removed by rinsing with 1x PBS and the media was replaced with serum free media. After 24 h, cell traction forces were recorded by imaging the fluorescent beads using a Leica DMI8 microscope, a Leica DFC9000 camera and a Lumencore Sola SEII LED light source at 37 °C with a 40x objective. Cells were then labeled with NucBlue (Fisher Scientific) live nuclear stain to determine the number of cells in the ensemble. After imaging, the cells were removed using RLT Lysis Buffer (Qiagen, Hilden, Germany). Cell traction forces were calculated using Fourier Traction Force Microscopy via a custom MATLAB (Mathworks, Natick, MA) software program[50].

Fluorescent Labeling of β-catenin and Vinculin. Cells were fluorescently labeled for vinculin (ab196454; Abcam, Cambridge, UK) and β-catenin (ab194119). Cells were fixed for 10 min with 4% formaldehyde in PBS at room temperature. Cells were then permeabilized with 0.3% TRX-100 for 5 min in PBS. Then, cells were blocked with 5% bovine serum albumen for 1 h. They were then stained simultaneously for vinculin and β-catenin for 2 h, both at 1:200 dilution ratios in 1XPBS.

Lung procurement. Native human whole lungs were acquired en bloc from brain-dead organ donors during transplant organ recovery through a research protocol with Gift of Life Michigan (Ann Arbor, MI). The University of Michigan Institutional Review Board has considered these approaches exempt from oversight because all subjects are deceased upon lung recovery. Tissues were procured from a Caucasian male with no history of smoking, diabetes or lung disease. The right middle lobe was dissected from the whole lung, and processed immediately for decellularization.

Decellularization. Lungs were decellularized as previously described to generate an acellular extracellular matrix scaffold[33]. Briefly, the airways were inflated with PBS containing antibiotics (10% penicillin/streptomycin, 4% amphotericin B, 2% gentamicin). Subsequently, a sequence of low concentration detergents and endonuclease (benzonase, Sigma) were applied within a physiological pH range (pH 7–8) at either 4 °C or room temperature. The decellularization protocol concluded with a final PBS buffer and benzonase rinse, and stored in PBS containing antibiotics.

Statistical testing. Sigmastat (Systat Software, San Jose, CA) was used to perform statistical tests. All pairwise comparisons used the t-test when the data was normally distributed. Otherwise, the Mann-Whitney test was used to compare the median values. The specific tests used, the number of samples, and the p-value are described along with the corresponding results. A p-value of 0.05 was used as the threshold for a statistically significant difference between data sets. For normally distributed data, we also calculated the statistical power of the test, which indicates the probability of avoiding a Type II error.

Data Availability

The datasets that support the findings of this study are available from the corresponding author on reasonable request.

References

1. Sears, M. R. *et al*. Regular inhaled beta-agonist treatment in bronchial asthma. *Lancet (London, England)* **336**, 1391–6 (1990).
2. Whelton, P. K. *et al*. 2017 ACC/AHA/AAPA/ABC/ACPM/AGS/APhA/ASH/ASPC/NMA/PCNA Guideline for the Prevention, Detection, Evaluation, and Management of High Blood Pressure in Adults: A Report of the American College of Cardiology/American Heart Association Task Force on Clinical Pr. *Hypertens. (Dallas, Tex. 1979)* **71**, e13–e115 (2018).
3. Severi, C. *et al*. Contribution of intestinal smooth muscle to Crohn's disease fibrogenesis. *Eur. J. Histochem.* **58**, 2457 (2014).
4. An, S. S. *et al*. Airway smooth muscle dynamics: a common pathway of airway obstruction in asthma. *Eur. Respir. J. Off. J. Eur. Soc. Clin. Respir. Physiol.* **29**, 834–60 (2007).
5. Briones, A. M., Arribas, S. M. & Salaices, M. Role of extracellular matrix in vascular remodeling of hypertension. *Curr. Opin. Nephrol. Hypertens.* **19**, 187–94 (2010).
6. Lemarié, C. A., Tharaux, P.-L. & Lehoux, S. Extracellular matrix alterations in hypertensive vascular remodeling. *J. Mol. Cell. Cardiol.* **48**, 433–9 (2010).

7. Bossé, Y., Riesenfeld, E. P., Paré, P. D. & Irvin, C. G. It's not all smooth muscle: non-smooth-muscle elements in control of resistance to airflow. *Annu. Rev. Physiol.* **72**, 437–462 (2010).
8. Bossé, Y., Chapman, D. G., Paré, P. D., King, G. G. & Salome, C. M. A 'Good' muscle in a 'Bad' environment: the importance of airway smooth muscle force adaptation to airway hyperresponsiveness. *Respir. Physiol. Neurobiol.* **179**, 269–275 (2011).
9. Venegas, J. G. *et al*. Self-organized patchiness in asthma as a prelude to catastrophic shifts. *Nature* **434**, 777–82 (2005).
10. Winkler, T. & Suki, B. Emergent structure-function relations in emphysema and asthma. *Crit. Rev. Biomed. Eng.* **39**, 263–80 (2011).
11. Wang, T., Wang, R., Cleary, R. A., Gannon, O. J. & Tang, D. D. Recruitment of β-catenin to N-cadherin is necessary for smooth muscle contraction. *J. Biol. Chem.* **290**, 8913–24 (2015).
12. Sun, Z., Martinez-Lemus, L. A., Hill, M. A. & Meininger, G. A. Extracellular matrix-specific focal adhesions in vascular smooth muscle produce mechanically active adhesion sites. *Am. J. Physiol. Cell Physiol.* **295**, C268–78 (2008).
13. Tang, D. D. Critical role of actin-associated proteins in smooth muscle contraction, cell proliferation, airway hyperresponsiveness and airway remodeling. *Respir. Res.* **16**, 134 (2015).
14. Tang, D. D. The Dynamic Actin Cytoskeleton in Smooth Muscle. *Adv. Pharmacol.* **81**, 1–38 (2018).
15. Stricker, J., Aratyn-Schaus, Y., Oakes, P. W. & Gardel, M. L. Spatiotemporal constraints on the force-dependent growth of focal adhesions. *Biophys. J.* **100**, 2883–93 (2011).
16. Yeh, Y.-C., Ling, J.-Y., Chen, W.-C., Lin, H.-H. & Tang, M.-J. Mechanotransduction of matrix stiffness in regulation of focal adhesion size and number: reciprocal regulation of caveolin-1 and β1 integrin. *Sci. Rep.* **7**, 15008 (2017).
17. Buckley, C. D. *et al*. Cell adhesion. The minimal cadherin-catenin complex binds to actin filaments under force. *Science* **346**, 1254211 (2014).
18. McCain, M. L., Lee, H., Aratyn-Schaus, Y., Kléber, A. G. & Parker, K. K. Cooperative coupling of cell-matrix and cell-cell adhesions in cardiac muscle. *Proc. Natl. Acad. Sci. USA* **109**, 9881–6 (2012).
19. Liu, Z. *et al*. Mechanical tugging force regulates the size of cell-cell junctions. *Proc. Natl. Acad. Sci. USA* **107**, 9944–9 (2010).
20. Tgavalekos, N. T. *et al*. Identifying airways responsible for heterogeneous ventilation and mechanical dysfunction in asthma: an image functional modeling approach. *J. Appl. Physiol.* **99**, 2388–2397 (2005).
21. Smiley-Jewell, S. M. *et al*. Three-dimensional mapping of smooth muscle in the distal conducting airways of mouse, rabbit, and monkey. *J. Appl. Physiol.* **93**, 1506–1514 (2002).
22. Strale, P.-O. *et al*. Multiprotein Printing by Light-Induced Molecular Adsorption. *Adv. Mater.* **28**, 2024–9 (2016).
23. Yoshie, H. *et al*. Traction Force Screening Enabled by Compliant PDMS Elastomers. *Biophys. J.* **114**, 2194–2199 (2018).
24. Wilson, J. W., Li, X. & Pain, M. C. The lack of distensibility of asthmatic airways. *Am. Rev. Respir. Dis.* **148**, 806–809 (1993).
25. Maruthamuthu, V., Sabass, B., Schwarz, U. S. & Gardel, M. L. Cell-ECM traction force modulates endogenous tension at cell-cell contacts. *Proc. Natl. Acad. Sci. USA* **108**, 4708–13 (2011).
26. Krishnan, R. *et al*. Reinforcement versus fluidization in cytoskeletal mechanoresponsiveness. *PLoS One* **4**, e5486 (2009).
27. An, S. S. *et al*. An inflammation-independent contraction mechanophenotype of airway smooth muscle in asthma. *J. Allergy Clin. Immunol.* **138**, 294–297.e4 (2016).
28. Mitrossilis, D. *et al*. Single-cell response to stiffness exhibits muscle-like behavior. *Proc. Natl. Acad. Sci. USA* **106**, 18243–8 (2009).
29. An, S. S. *et al*. Cell stiffness, contractile stress and the role of extracellular matrix. *Biochem. Biophys. Res. Commun.* **382**, 697–703 (2009).
30. Parameswaran, H., Lutchen, K. R. & Suki, B. A computational model of the response of adherent cells to stretch and changes in substrate stiffness. *J. Appl. Physiol.* **116**, 825–34 (2014).
31. Zeng, G., Apte, U., Cieply, B., Singh, S. & Monga, S. P. S. siRNA-mediated beta-catenin knockdown in human hepatoma cells results in decreased growth and survival. *Neoplasia* **9**, 951–9 (2007).
32. Araujo, B. B. *et al*. Extracellular matrix components and regulators in the airway smooth muscle in asthma. *Eur. Respir. J. Off. J. Eur. Soc. Clin. Respir. Physiol.* **32**, 61–9 (2008).
33. Balestrini, J. L. *et al*. Production of decellularized porcine lung scaffolds for use in tissue engineering. *Integr. Biol. (Camb).* **7**, 1598–610 (2015).
34. Kamm, R. D. *Airway Wall Mechanics*. 47–72 (1999).
35. An, S. S. *et al*. Stiffness changes in cultured airway smooth muscle cells Stiffness changes in cultured airway smooth muscle cells, https://doi.org/10.1152/ajpcell.00425.2001 (2012).
36. Harvey, B. C., Parameswaran, H. & Lutchen, K. R. Can breathing-like pressure oscillations reverse or prevent narrowing of small intact airways? *J. Appl. Physiol.* **119**, 47–54 (2015).
37. Pini, L. *et al*. Differences in proteoglycan deposition in the airways of moderate and severe asthmatics. *Eur. Respir. J. Off. J. Eur. Soc. Clin. Respir. Physiol.* **29**, 71–77 (2007).
38. Kong, F., García, A. J., Mould, A. P., Humphries, M. J. & Zhu, C. Demonstration of catch bonds between an integrin and its ligand. *J. Cell Biol.* **185**, 1275–84 (2009).
39. Lele, T. P. *et al*. Mechanical forces alter zyxin unbinding kinetics within focal adhesions of living cells. *J. Cell. Physiol.* **207**, 187–94 (2006).
40. Bates, J. H. T. & Maksym, G. N. Mechanical determinants of airways hyperresponsiveness. *Crit. Rev. Biomed. Eng.* **39**, 281–96 (2011).
41. Irons, L., Owen, M. R., O'Dea, R. D. & Brook, B. S. Effect of Loading History on Airway Smooth Muscle Cell-Matrix Adhesions. *Biophys. J.* **114**, 2679–2690 (2018).
42. Park, C. Y. *et al*. High-throughput screening for modulators of cellular contractile force. *Integr. Biol. (Camb).* https://doi.org/10.1039/c5ib00054h (2015).
43. Polio, S. R. *et al*. Topographical control of multiple cell adhesion molecules for traction force microscopy. *Integr. Biol. (Camb).* **6**, 357–65 (2014).
44. Polio, S. R., Rothenberg, K. E., Stamenović, D. & Smith, M. L. A micropatterning and image processing approach to simplify measurement of cellular traction forces. *Acta Biomater.* **8**, 82–8 (2012).
45. Krishnan, R. *et al*. Substrate stiffening promotes endothelial monolayer disruption through enhanced physical forces. *Am. J. Physiol. Cell Physiol.* **300**, C146–54 (2011).
46. Kim, J.-H. & Asthagiri, A. R. Matrix stiffening sensitizes epithelial cells to EGF and enables the loss of contact inhibition of proliferation. *J. Cell Sci.* **124**, 1280–1287 (2011).
47. Sim, J. Y. *et al*. Spatial distribution of cell-cell and cell-ECM adhesions regulates force balance while main-taining E-cadherin molecular tension in cell pairs. *Mol. Biol. Cell* **26**, 2456–65 (2015).
48. Hiorns, J. E., Jensen, O. E. & Brook, B. S. Nonlinear compliance modulates dynamic bronchoconstriction in a multiscale airway model. *Biophys. J.* **107**, 3030–3042 (2014).
49. Politi, A. Z. *et al*. A multiscale, spatially distributed model of asthmatic airway hyper-responsiveness. *J. Theor. Biol.* **266**, 614–24 (2010).
50. Butler, J. P., Tolić-Nørrelykke, I. M., Fabry, B. & Fredberg, J. J. Traction fields, moments, and strain energy that cells exert on their surroundings. *Am. J. Physiol. Cell Physiol.* **282**, C595–605 (2002).

Acknowledgements
We acknowledge the assistance provided by Dr. Peter Novak, statistical consultant at Harvard Medical School, Boston MA. This work was supported by NIH grants HL129468 and HL122513 (HP), and HL123552 (RK).

Author Contributions
H.P., R.K., J.B. and S.P. contributed to the experimental design, S.P., R.R.J., J.B. and S.S. conducted the experiments, S.S., S.P., R.R.J., R.K., J.B. and H.P. analysed the results. All authors contributed to manuscript preparation.

Additional Information
Competing Interests: The authors declare no competing interests.

Publisher's note: Springer Nature remains neutral with regard to jurisdictional claims in published maps and institutional affiliations.